Corrosion Characteristics of Ni-Based Hardfacing Alloy Deposited on Stainless Steel Substrate by Laser Cladding

REENA AWASTHI, GEOGY ABRAHAM, SANTOSH KUMAR, KAUSTAVA BHATTACHARYYA, NACHIKET KESKAR, R.P. KUSHWAHA, RAMANA RAO, R. TEWARI, D. SRIVASTAVA, and G.K. DEY

In this study, corrosion characteristics of a nickel-based Ni-Mo-Cr-Si hardfacing alloy having 32Mo, 15Cr, and 3Si (wt pct) as alloying elements, deposited on stainless steel SS316L substrate by laser cladding, have been presented. Corrosion behavior of the laser clad layer was evaluated in reducing (0.1 M HCl) and oxidizing (0.5 M HNO_3) environments, in comparison with the reference substrate SS316L, using electrochemical potentiodynamic technique at room temperature. The corrosion mechanisms have been evaluated on the basis of microstructural and microchemical analysis using scanning electron microscopy attached with energy-dispersive spectrometry. Passivity behavior of the laser clad layer was studied in 0.5 M H_2SO_4, using the potentiostatic technique and analyzing the passive layer by X-ray photoelectron spectroscopy. Laser clad layer of Ni-Mo-Cr-Si exhibited higher pitting corrosion resistance in chloride (reducing) environment, indicated by much higher breakdown potential (~0.8 V_{SCE}) and the absence of pitting as compared to substrate SS316L (~0.3 V_{SCE}). However, in oxidizing (0.5 M HNO_3) environment, both the laser clad layer and substrate SS316L showed excellent and similar corrosion resistance exhibiting high breakdown potential (~0.85 V_{SCE}) and wide passivation range (~0.8 V_{SCE}) with low passive current density (~4 to 7 $\times$ 10^{-6} A/cm^2). The stable passive layer formed on laser clad layer of Ni-Mo-Cr-Si after exposure in 0.5 M H_2SO_4 solution at constant potential ~0.6 V_{SCE} (within the passive range), consisted oxides of Mo as Mo^{+4} (MoO_2) and Mo^{+6} $(MoO_4)^{-2}$, Cr as Cr^{3+} (mixture of both Cr_2O_3 and Cr $(OH)_3$), and Si as Si^{4+}(SiO_2), which have contributed to passivation and repassivation and therefore excellent corrosion behavior.

DOI: 10.1007/s11661-017-4074-1

I. INTRODUCTION

WEAR and corrosion are the most common surface-initiated failure mechanisms for the components working under aggressive conditions. When components are exposed to corrosion environments, combined effects of corrosion and wear are much more detrimental than those caused by corrosion or wear alone.[1,2] In order to improve wear and corrosion resistance of the surface, a large variety of hardfacing alloys, including cobalt (Co), nickel (Ni) and iron (Fe)-based, have been developed and explored, by depositing on various substrates.[3,4] Of these hardfacing alloys, some alloys provide excellent wear resistance but poor resistance to corrosive environments (such as carbon containing Fe-based hardfacing alloys, metal/ceramic composites to name a few) and *vice-versa* (Ni-based alloys such as Inconel and Monel). Generally, increase in hardness and wear resistance of the hardfacing alloy is associated with the reduction in corrosion resistance.[5] This behavior has been attributed to the fact that most of the materials derive their wear resistance from the presence of a hard phase (carbide, boride, or intermetallic phase) dispersed in a relatively more ductile eutectic or solid solution matrix. The presence of multiphases in hardfacing alloys with different compositions may sometime lead to preferential partitioning of some of the corrosion-resistant elements such as chromium (Cr) in one of the phases and make the other phase prone to corrosion. Generally, carbide containing wear-resistant hardfacing alloys, most specifically metal/ceramic composites (*e.g.*, WC-Co) is not corrosion-resistant.[6] Generally, the susceptibility of Co binder to chemical attack limits the corrosion resistance of most commonly used Co-based carbide containing hardfacing alloys. The corrosive media dissolve the Co binder from the matrix, and thus a weak, unsupported skeleton of tungsten carbide grains left behind gets abraded away easily.[6]

REENA AWASTHI, GEOGY ABRAHAM, SANTOSH KUMAR, NACHIKET KESKAR, R.P. KUSHWAHA, R. TEWARI, D. SRIVASTAVA, and G.K. DEY are with the Material Science Division, Laser Materials Processing Section, Bhabha Atomic Research Centre, S-63 A, South Site, Mumbai, Maharastra 400085, India. Contact e-mail: reena@barc.gov.in KAUSTAVA BHATTACHARYYA is with the Chemistry Division, Bhabha Atomic Research Centre, Mumbai, India. RAMANA RAO is with the Materials Characterisation Division, Nuclear Fuel Complex, Hyderabad, India.
Manuscript submitted September 8, 2016.
Article published online March 24, 2017

Co- and Ni-based Tribaloy series of intermetallic alloys, containing 32Mo, 15Cr, and 3Si (wt pct) as alloying elements, exhibit their superiority over other hardfacing alloys in terms of their overall resistance to both wear and corrosion over a wide range of temperatures [~1073 K to 1273 K (~800 °C to 1000 °C)].[7–9] These alloys are primarily strengthened by Mo-rich intermetallic Laves phase dispersed in a Co- or Ni-based gamma solid solution or a eutectic matrix.[10–12]

Ni-based intermetallic Laves phase alloy Ni32Mo15Cr3Si (Tribaloy T-700) is the only Ni-based alloy among all the Tribaloy series of alloys, which has been described as an alternative to costly and unsuitable Co-based hardfacing alloy for nuclear applications.[13,14] Corrosion behavior of Ni-Mo-Cr-Si alloy in as-cast, weld-overlaid, and thermally sprayed conditions has been studied in different environments.[9,15–18]

Demo *et al.*[9] have demonstrated that Ni32Mo15Cr3Si exhibits superior wear performance as compared to several stainless steels and Ni-based alloys and is suitable for the sliding surfaces or movable shafts inside cylindrical bushings, bearing valves, and seals exposed to both oxidizing (ferric chloride, nitric acid) and reducing (hydrochloric acids) acidic corrosive environments.

Bolelli *et al.*[15,16] have shown that the as-sprayed and heat-treated High Velocity Oxy-fuel (HVOF) deposited Ni-Mo-Cr-Si coatings exhibited high current density ~10^{-4} A/cm^2 in the passive-like stage in 0.1 M HCl solution. Thus, it did not display ideal perfect passive stage, which requires much lower current density ~10^{-6} A/cm^2, because of the presence of defects such as porosities, unmelted particles, and oxide inclusions, which are generally inherent to thermally sprayed coatings.

Johnson *et al.*[17,18] have evaluated the friction, wear, and corrosion performance of several metallurgical coatings including chromium carbide, nickel aluminide, and Tribaloy T-700, deposited by various processes including detonation gun (DG) and plasma spray (PS), in sodium environment, in 473 K to 923 K (200 °C to 650 °C) temperature range. Tribaloy T-700 has consistently exhibited the best performance in the fast breeder reactor environment. The coatings deposited by DG exhibited lower friction, wear, and corrosion rates than those deposited by PS.

In general, the coatings deposited by thermal spraying techniques (HVOF, PS) do not show good corrosion performance due to the presence of defects such as porosity and oxide inclusion even when noble alloys are deposited. Therefore, there is a need of either post-deposition modification of the thermally sprayed coatings or of a deposition process that produces sound and defect-free coatings, strongly bonded to the substrate. In this regard, laser cladding has shown its superiority over other conventional surfacing techniques in terms of microstructure, wear, and most specifically corrosion behavior.[19,20] Laser remelting of thermally sprayed coatings leads to densification and elimination of the defects such as porosity and oxide inclusions, generally present in thermally sprayed coatings.[21,22] Laser processing was found to achieve minimum variation in deposit thickness along with strong fusion bond (unlike mechanical anchoring in thermal spraying) between the clad layer and the substrate while maintaining a low dilution of clad alloy with the substrate (unlike high dilution in weld surfacing). These contradictory requirements of strong fusion bond and low dilution could be simultaneously achieved, because of precise and controlled delivery of the laser beam and coating material to the process zone. This makes laser cladding process unique and superior as compared to other conventional techniques for deposition of coatings. In addition, rapid solidification associated with laser cladding results in extended solid solubility, formation of metastable phases, and fine microstructure, leading to improved metallurgical, wear, and corrosion properties of the coatings. Low heat input associated with laser cladding leads to low distortion of the components.[23]

Published literature on corrosion behavior of Ni32Mo15Cr3Si alloy coating, deposited by laser cladding is scarcely reported. In order to evaluate the corrosion performance of laser-deposited Ni32Mo15Cr3Si alloy coating, systematic corrosion studies have been carried out in both reducing (0.1 M HCl) and oxidizing (0.5 M HNO_3) environments using potentiodynamic technique. For the purpose of comparison, the substrate SS316L has also been evaluated for its corrosion resistance in the given environments. Passivity behavior of the laser clad layer was studied in 0.5 M H_2SO_4 using the potentiostatic technique and passive layer was analyzed by X-ray photoelectron spectroscopy (XPS). Differences in the corrosion behavior of laser clad layer and the substrate (SS316L) have also been discussed based on the microstructural and microchemical analyses performed using SEM-EDS. Hereafter, the particular alloy Ni32Mo15Cr3Si used as a hardfacing alloy in the present study will be referred as Ni-Mo-Cr-Si alloy for convenience.

II. EXPERIMENT

Laser cladding was carried out using high-power continuous wave Nd-YAG laser (Make: Trumpf Laser, Germany; Model: HL1006D) using blown powder method, where the alloy powder was fed coaxially with the laser beam using a powder feeder (Make: Sulzer-Metco, Switzerland; Model: Twin 10C). Clad layers were produced over a wide range of process variables as listed in Table I to optimize the parameter range to produce defect-free clad layer of Ni-Mo-Cr-Si alloy, with low dilution (~10 pct) and sound metallurgical bond with SS316L substrate. Laser beam spot diameter was kept constant (~2 mm) in all these experiments. Argon gas was used as the carrier gas for delivery of clad alloy powder to the process zone and also as the shielding gas to protect the melt pool from oxidation.

The optimized set of process parameters was derived by analyzing the cross-section macrograph of single clad track, produced over the entire range of process parameters explored in this study (Table I), which resulted in defect (crack, porosity)-free clad layers of Ni-Mo-Cr-Si alloy, metallurgically bonded with the

Table I. Range of Process Variables Used in the Laser Cladding Experiments

SI. No.	Process Variables	Range
1	laser power (P)	600 to 1000 W
2	travel speed (TS)	100 to 800 mm/min
3	powder feed rate (PFR)	5 to 35 gm/min
4	spot diameter of laser beam	~2 mm constant

substrate (SS316L) with low dilution (~10 to 15 pct). Optimized set of process parameters was used to produce larger areas by overlapping several adjacent tracks side by side with an overlapping of ~50 pct between adjacent tracks, to evaluate corrosion behavior of the clad layer.

Corrosion behavior of the laser clad layer was evaluated by electrochemical polarization tests (Make: ACM instruments, Model: Gill AC potentiostat), in both reducing (0.1 M HCl) and oxidizing (0.5 M HNO_3) environments. These tests were also conducted with the substrate material SS316L for the purpose of comparison. The samples were spot-welded with a steel wire to make electrical contact and a plastic sleeve was placed over the wire as insulation. The samples were ground using SiC papers of different grit sizes up to 1200 for final finish. One square centimeter area of the surface of the mounted sample was exposed to the solution by covering rest of the area with lacquer, to avoid any crevice effect.

The tests were carried out in a conventional three-electrode cell. The test sample was referred as the working electrode and a saturated calomel electrode (SCE) as the reference electrode at constant potential, against which the potential of test sample was measured. Platinum foil was used as an auxiliary electrode to supply current and control the potential of the working electrode. Prior to each experiment, deaeration of the electrolyte was carried out by purging argon gas for half an hour in order to remove dissolved oxygen from the solution. The purging was continued throughout the experiment as well. The sample was introduced into the purged solution and the open circuit potential (OCP) value was stabilized for half an hour. Tests were initiated only after attaining steady-state open circuit potential (OCP). Tafel technique[24] was employed with a voltage scan from a 100 mV offset from OCP as initial voltage to a final voltage till transpassive region (~1.2 V_{SCE}) at a scan rate of 0.0005 V/s. The corrosion current density (i_{corr}) and corrosion potential (E_{corr}) were calculated using Tafel analysis using the data obtained from cathodic and anodic polarization curves.[24] Corroded surface of the samples was also characterized using an optical microscope and SEM-EDS to study the corrosion mechanisms. Potentiostatic experiments at a potential within the passive range (~0.6 $V_{SCE,}$ as established by taking potentiodynamic polarization run in 0.5 M H_2SO_4 solution) were carried out in 0.5 M H_2SO_4 solution to study passivation behavior of the Ni-Mo-Cr-Si alloy laser clad layer. The surface film was analyzed using X-ray photoelectron spectroscopy (XPS) which was carried out using the SPECS instrument with a PHOBIOS 100/150 Delay Line Detector (DLD) with 385 W, 13.85 kV, and 175.6 nA. Al Kα (1486.6 eV) dual anode was used as the X-ray source. The XPS was taken with transmission pass energy of 50 eV. As an internal reference for the absolute binding energy, the C-1s peak (284.5 eV) was utilized. Initially, the XPS unit was calibrated using Au $4f_{7/2}$ line at 83.98 eV from a specimen of Au film. A value of 83.977 eV was obtained. The data obtained from the instrument were processed using the CASA software. The survey peak of the specimens was initially corrected for the C-1s peak. The quantitative estimate for the elemental analysis was performed. High-resolution XPS spectra were also initially calibrated against the C-1s peak (284.5 eV). After that, these were deconvoluted using the CASA software, developed by Fairley,[25] for the presence of the different electronic states of the particular element. The baseline correction for each spectrum was initially carried out using a Shirley background correction.[26] The deconvolution was carried out using a linear combination of Gaussian (30 pct) and Lorentzian (70 pct), in order to find out the chemical state and compound of main elements present in the passive layer. The XPS signals were separated based on the contributions from the different elements present in the alloy. The binding energies of all elements and their compounds are referred to using standard tables published by VG-XPS instrumentation Co., Ltd as well as confirmed with the published literature.

III. RESULTS

Based on the analysis of the clad track cross sections, produced over the entire range of process parameters (Table I), it was observed that the most common defect in Ni-Mo-Cr-Si alloy laser clad layer was crack. Cracks were primarily observed at higher PFR (>20 gm/min) and at either too low (≤100 mm/min) or high TS (≥800 mm/min), specifically during the overlapping pass. Higher PFR beyond a certain threshold (>20 gm/min) also resulted in rapid increases in the height of the clad layer and subsequently small aspect ratio (width to height ratio <1.5) as well as parabolic shape of the clad layer, which may increase the risk of inter-run porosity during overlapping passes for large area coverage.[23] It was also observed that the increase in the travel speed beyond certain threshold (~800 mm/min) resulted in very thin clad layer (<500 μm) and poor metallurgical bonding, due to reduced interaction time of laser beam with the powder and the substrate. Additionally, it was found that laser power ~1000 W (at ~2 mm spot size of the laser beam) resulted in more dilution (>25 pct) of clad layer with substrate, which

was not desirable. Thus, based on these observations of entire clad track cross sections, optimized set of process parameters for producing defect-free clad layers Ni-Mo-Cr-Si alloy, metallurgically bonded with the substrate (SS316 L) with low dilution (~10 to 15 pct) is listed in Table II.

Laser clad layer of Ni-Mo-Cr-Si alloy produced by overlapping of tracks side by side with an overlapping of ~50 pct between adjacent tracks, at one of the optimized parameters, is shown in Figure 1.

A. *Microstructure of the Clad Layer, Before Exposing to Corrosive Environment*

Microstructures of the substrate/clad interfacial region and top surface of the Ni-Mo-Cr-Si alloy clad layer produced at the above optimized parameter, before exposing to corrosive environment, are shown in Figures 2(a) and (b), respectively.

The laser clad layer (thickness ~1 mm) was defect-free and metallurgically bonded with the substrate SS316L (Figure 2(a)). Mode of solidifications varied from planar at the fusion line, to cellular and then to dendritic toward the surface of the clad layer (Figure 2(a)), primarily dictated by decreasing thermal gradient (G) and increasing solidification rate (R) from interface upward, *i.e.*, decreasing G/R ratio. The clad surface layer (Figure 2(b)) exhibited the presence of two phases. Compositions of the phases are shown in Table III. Thus, the clad layer consisted of primary dendrites of Mo-rich phase dispersed in the softer Ni-based (Table III) gamma solid solution or lamellar eutectic phase mixture of both (Figure 2(b)). The clad layer at the surface exhibited low dilution (~10 to 15 pct) confirmed by EDS.

X-ray diffraction analysis (Figure 3) carried on the surface of the clad layer (before exposing to corrosive environment) showed the presence of primary hexagonal close-packed (HCP) intermetallic laves phase (Mo-rich bright phase (Figure 2(b)) dispersed in the Ni-based γ solid solution (Ni-rich gray phase (Figure 2(b)) of face-centered cubic (FCC) crystal structure.

B. *Electrochemical Corrosion Studies in HCl Environment*

The potentiodynamic polarization curves for Ni-Mo-Cr-Si laser clad layer and SS316L substrate exposed in 0.1 M HCl solutions (a reducing acid) are shown in Figure 4. Table IV summarizes the electrochemical polarization test results showing the values of corrosion current density (i_{corr}) and corrosion potential (E_{corr}), calculated using the Tafel technique in HCl environment[24] and breakdown potential (Figure 4). The error in measurement is within ±5 pct of the measured value.

Laser clad layer of Ni-Mo-Cr-Si alloy showed higher breakdown potential (~0.8 V_{SCE}) after exposing in 0.1 M HCl solutions, as compared to the substrate SS316L (Figure 4), which showed much lower breakdown (pitting) potential (~0.3 V_{SCE}). Lower pitting potential indicated higher susceptibility for pitting corrosion in SS316L as compared to Ni-Mo-Cr-Si laser clad layer in chloride environment. The pitting resistance equivalent number (PREN) was calculated for the clad alloy and stainless steel using the relation (PREN = pctCr + 3.3 pctMo + 17 pctN).[19,24] The calculated PREN values for Mo-rich phase and Ni-based gamma solid solution phase in clad alloy are 150 and 83, respectively. The resistance to pitting corrosion in a multiphase alloy is governed by the phase with the lowest PREN value, *i.e.*, 83 for Ni-based gamma solid solution in case of laser clad layer. The PREN value of SS316L substrate was 27. Thus, higher PREN number for laser clad Ni-Mo-Cr-Si layer (PREN No. 83) represents higher pitting corrosion resistance as compared to substrate SS316L (PREN No.27). The current density corresponding to passive region was low, in the range of 10^{-6} to 10^{-5} A/cm^2, for both SS316L and laser clad Ni-Mo-Cr-Si layer (Figure 4).

In addition, lower and nearly identical corrosion current density (i_{corr} ~10^{-7} A/cm^2) for both the substrate and clad layer (Table IV) confirms that the laser clad layer as well as the substrate SS316L is corrosion-resistant in the given medium, whereas the E_{corr} values were different for both the alloys with the laser clad layer of Ni-Mo-Cr-Si showing a little higher active potential as compared to SS316L. However, passivity region is larger (~0.755 V_{SCE}) for laser clad layer as compared to the substrate SS316L (~0.28 V_{SCE}) indicating a more stable passive film.

Optical and SEM micrographs of the corroded surface for Ni-Mo-Cr-Si laser clad layer and SS 316L substrate, after polarizing beyond breakdown potential, in 0.1 M HCl solutions are shown in Figures 5 and 6, respectively.

Laser clad layer of Ni-Mo-Cr-Si alloy did not undergo pitting and displayed etched structure (Figures 5(a) through (c)) after polarizing beyond breakdown potential in 0.1 M HCl solution. Selective dissolution of eutectic matrix or gamma solid solution phase (Ni-rich gray phase) as compared to Mo-rich intermetallic Laves phase (white) in laser clad layer is shown (Figures 5(b) and (c)). Less corroded Mo-rich

Table II. Optimum Range of Process Parameters for Producing Defect-Free Clad Layer

Sl. No.	Process Variables	Range
1.	laser power (P)	600 to 800 W
2.	travel speed (TS)	200 to 600 mm/min
3.	powder feed rate (PFR)	5 to 20 gm/min

intermetallic Laves phase protrudes out of the corroded matrix with lower Mo content (Figure 5(c)), whereas extensive corrosion damage by pitting was observed in substrate SS316 as shown in Figures 6(a) and (b) after polarizing beyond breakdown or pitting potential in 0.1 M HCl.

C. *Electrochemical Corrosion Studies in HNO_3 Environment*

The electrochemical polarization curves for Ni-Mo-Cr-Si laser clad layer and SS316L substrate in 0.5 M HNO_3 solutions (an oxidizing acid) are shown in Figure 7. Both the laser clad layer of Ni-Mo-Cr-Si alloy and substrate SS316L exhibited higher breakdown (transpassive) potential (~0.85 V_{SCE}) in 0.5 M HNO_3 solution (Figure 7). The passive current density was low and nearly in the same range for both SS 316L and laser clad Ni-Mo-Cr-Si layer (~4 to 7 $\times$ 10^{-6} A/cm^2), which confirms that both the alloys are adequately passive. Thus, nearly similar corrosion behavior was observed for both laser clad Ni-Mo-Cr-Si alloy and substrate SS316L, when exposed to 0.5 M HNO_3 solution.

SEM micrographs of the exposed surface for laser clad layer and SS 316L substrate in 0.5 M HNO_3 solutions are shown in Figures 8 and 9, respectively. Both the laser clad layer and substrate SS316L showed excellent passivity in the nitric acid environment (Figures 8 (a) and (b) and 9). Exposed surface of the laser clad Ni-Mo-Cr-Si alloy displayed etched structure with preferential dissolution (Figure 8(b)) of solid solution matrix (gray) as compared to Mo-rich intermetallic Laves phase (white) since electrochemical measurement was done beyond the transpassive potential, whereas preferential dissolution was not observed in the case of SS316 as the microstructure is more homogenous (Figure 9).

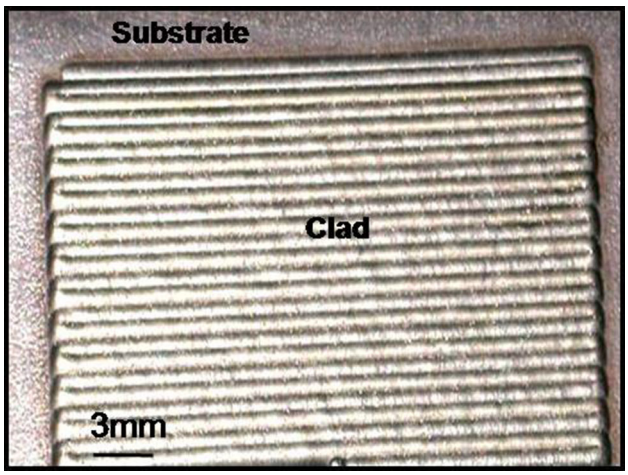

Fig. 1—As-deposited clad layer (laser power: 800 W, speed: 200 mm/min powder feed rate: 8.3 gm/min).

D. *Analysis of the Passive Film Formed on Ni-Mo-Cr-Si Laser Clad Layer in 0.5 M H_2SO_4*

Figure 10 shows the potentiostatic curve for the laser clad layer of Ni-Mo-Cr-Si alloy, at a constant potential

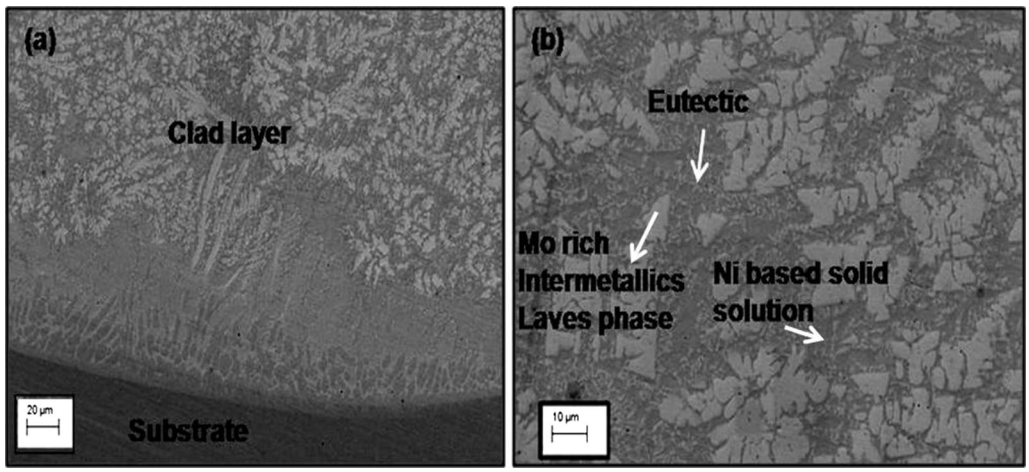

Fig. 2—SEM micrographs before exposing to corrosive environment showing (*a*) sound metallurgical bond between the laser clad layer of Ni-Mo-Cr-Si alloy and the substrate SS316L (*b*) microstructure of the clad top surface consisting primary dendrites of molybdenum (Mo)-rich phase dispersed in the softer nickel (Ni)-based gamma solid solution or lamellar eutectic phase mixture of both.

Table III. Composition of the Phases Present in Top Surface of the Ni-Mo-Cr-Si Alloy Clad Layer Before Exposing to Corrosive Environment

Elements	Ni	Mo	Cr	Si	Fe
Mo-rich phase (bright) (wt pct)	36.2	41.4	14.2	4.5	2.8
Ni-based gamma solid solution (gray) phase (wt pct)	53.9	19.1	19.7	2.1	4.7

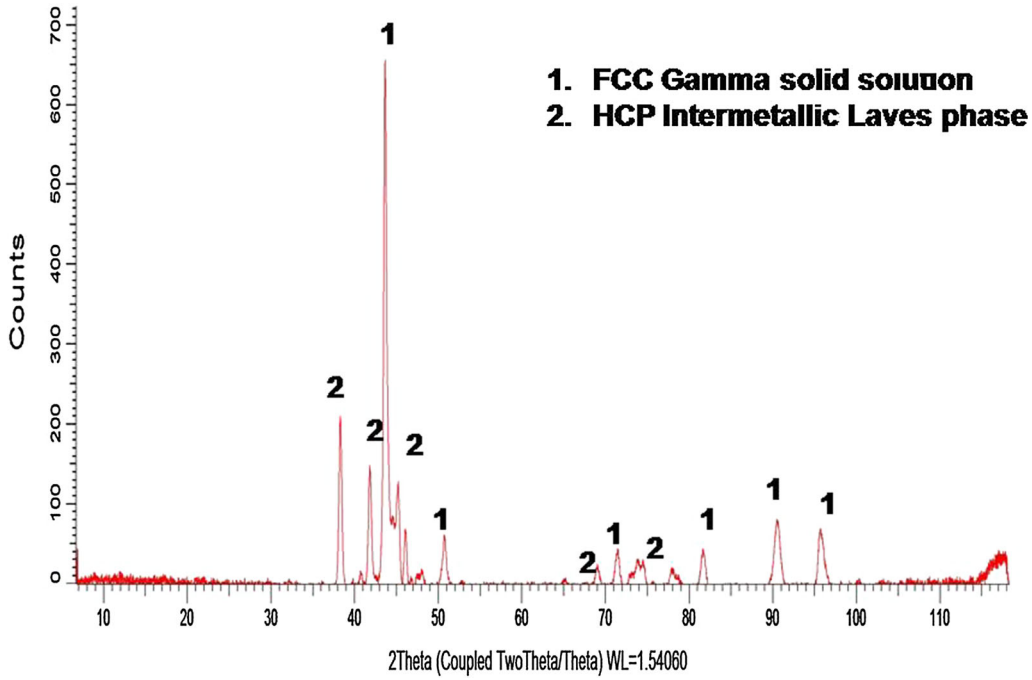

Fig. 3—XRD pattern of the laser clad surface layer of Ni-Mo-Cr-Si alloy (before exposing to corrosive environment), showing the presence of two phases (1) hexagonal close-packed (HCP) intermetallic Laves phase (2) face-centered cubic (FCC) gamma solid solution.

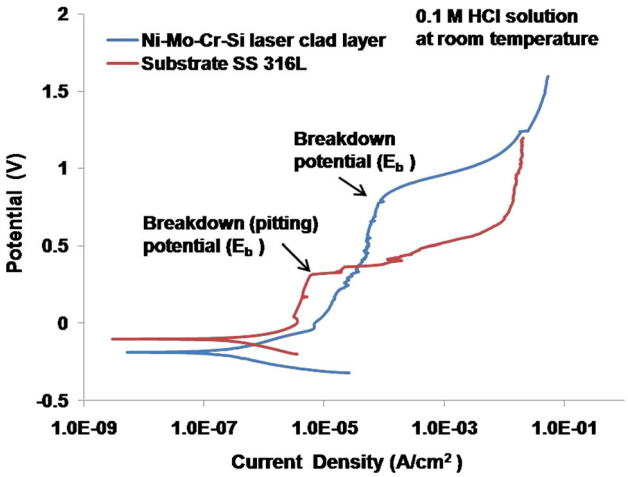

Fig. 4—Electrochemical polarization curve, showing the localized corrosion behavior of laser clad layer of Ni-Mo-Cr-Si and substrate SS316L after exposure in 0.1 M HCl solution.

Table IV. Electrochemical Polarization Test Results for Ni-Mo-Cr-Si Laser Clad Layer and Substrate SS316L After Exposure in 0.1 M HCl Solutions: Corrosion Current Density (i_{corr}), Corrosion Potential (E_{corr}), Breakdown Potential (E_b)

Alloy	E_b (V_{SCE})	i_{corr} (A/cm^2)	E_{corr} (V_{SCE})
Ni-Mo-Cr-Si laser clad layer	0.8	1.48×10^{-7}	−0.184
Wrought SS-316 L	0.3	1.99×10^{-7}	− 0.103

of ~0.6 V_{SCE} within the passive regime, as established by taking potentiodynamic polarization run in 0.5 M H_2SO_4 solution.

It showed stable current density value over the passivation time of 1 hour at 0.6 V_{SCE}, indicating the stability of the passive film formed on Ni-Mo-Cr-Si laser clad layer. The initial high current density indicated that the alloy has a film-free surface which reacted with the environment to form a passive layer. This passive layer tends to form within 1 minute of the exposure at the given potential in 0.5 M H_2SO_4.

A survey scan of the passive layer formed on laser clad layer of Ni-Mo-Cr-Si alloy obtained by X-ray photoelectron spectroscopy (XPS) is presented in Figure 11.

The survey scan showed the presence of XPS peaks of Ni-2p, Cr-2p, Mo-3p, Mo-3d, C-1s, O-1s, and Si-2p and their corresponding Auger peaks for Cr_{LMM}, Ni_{LMM}, O_{KLL}, C_{KLL}, Si_{LMM}, and Mo_{MNV}. Quantitative measurement of the elements, measured using the CASA software, showed the presence of Mo (13.7 at. pct), Cr (2.38 at. pct), Si (5.06 at. pct), and O (76.96 at. pct) in the passive layer. Presence of O-1s peak could be due to the formation of respective oxide of the alloying elements or due to the presence of adsorbed oxygen/H_2O on the surface of the alloy or formation of respective hydroxide species. However, only adsorption process (either of O_2 or H_2O) or formation of hydroxides could in no ways explain the presence of such a large amount of O-1s. Therefore, it is quite perceivable that the elements of this alloy have formed their respective oxides. The above result showed that the contribution from Mo was the highest in the formation of the oxide followed by Si and Cr. The oxides of alloying element Ni in the passive layer were negligibly low.

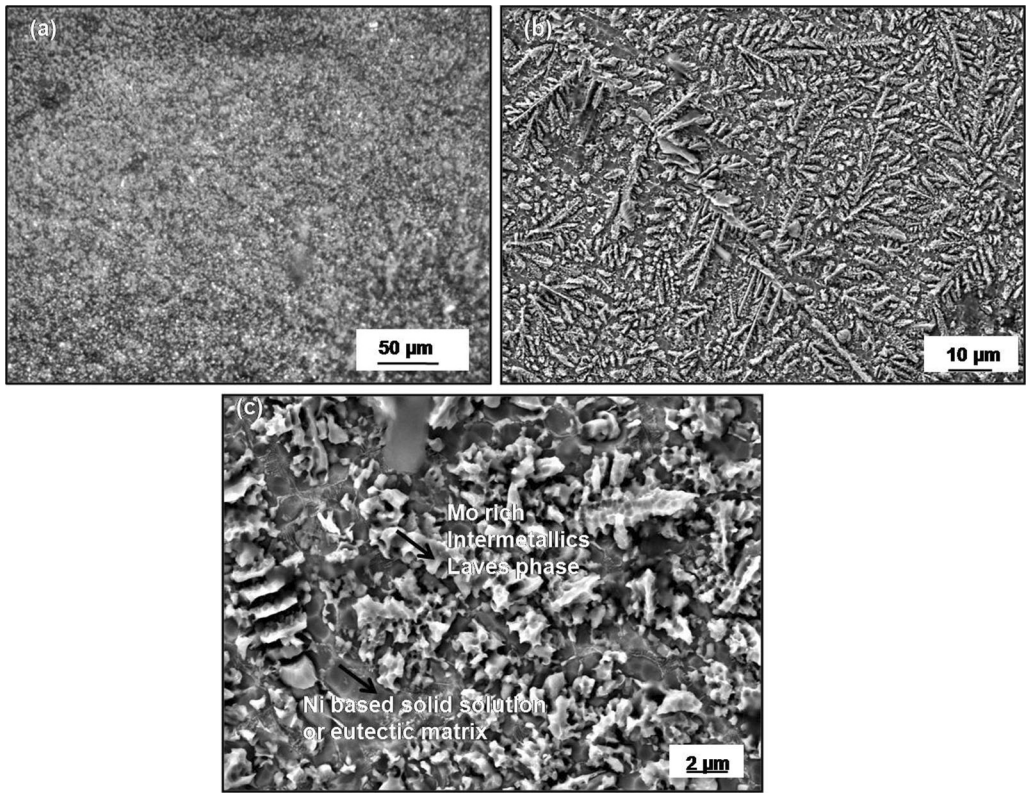

Fig. 5—Optical (*a*), SEM micrograph (*b*, *c*) of laser clad layer of Ni-Mo-Cr-Si after polarizing beyond breakdown potential (~0.8 V_{SCE}) in 0.1 M HCl solutions, showing etched structure with selective leaching or corrosion of eutectic matrix or gamma solid solution phase (gray) as compared to Mo-rich intermetallic Laves phase (bright) and absence of pits.

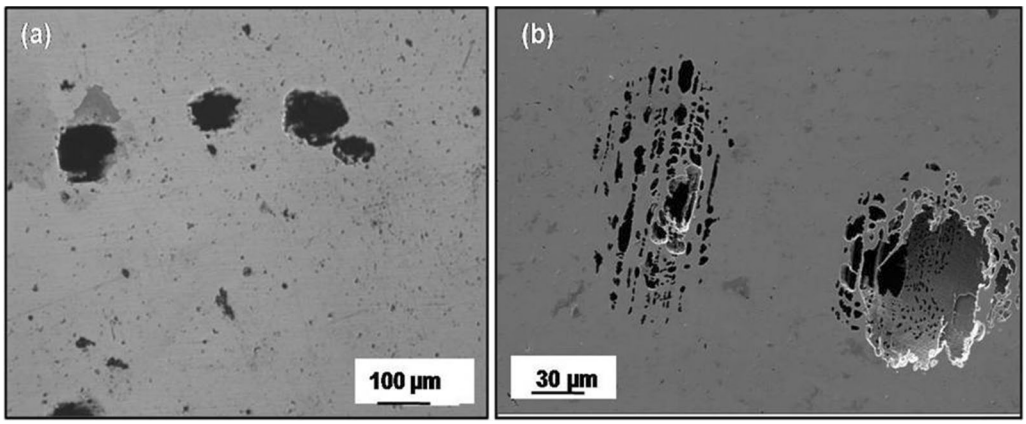

Fig. 6—Microstructure of SS316L after electrochemical polarization beyond breakdown (pitting) potential (~0.3 V_{SCE}) in 0.1 M HCl (*a*) Optical and (*b*) SEM micrograph, showing extensive pitting.

High-resolution spectra with deconvoluted peaks of the main elements are presented in Figures 12(a) through (d).

The deconvoluted peak of O-1s (Figure 12(a)) showed the presence of four peaks corresponding to binding energy (B.E) values of 533.01, 531.2, 530.29, and 529.04 eV. The O-1s peaks from 529 to 531 eV could be assigned to the lattice oxide peaks and the peak at 533.01 eV could be assigned to the hydroxides (OH^-) of alloying element, which are consistent with the literature.[27–30] The three deconvoluted peaks of O-1s corresponding to 531.2, 530.29, and 529.04 eV could be due to the formation of the oxides of Mo, Cr, and Si present in different proportions in oxide layer.

The $Mo_{3d5/2}$ XPS peak could be deconvoluted into three components corresponding to binding energy values of 229.03, 229.84, and 228.4 eV, as shown in Figure 12(b).

These peaks could be interpreted as different oxidation states of Mo (Mo^{+4}, Mo^{+6}, and Mo^0). The peak corresponding to 228.4 eV represents the metallic Mo (Mo^0) which is mostly the unreacted Mo present in the

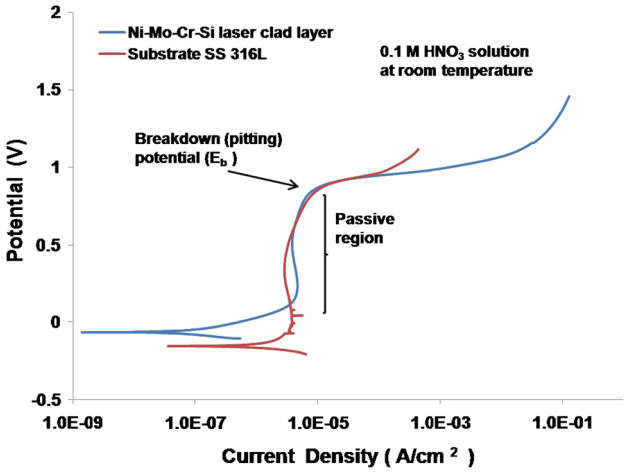

Fig. 7—Electrochemical polarization curve, showing the passivity behavior of Ni-Mo-Cr-Si laser clad layer and SS316L substrate after exposure in 0.5 M HNO_3 acid solution.

alloy. The peak at 229.03 eV represents Mo^{4+} which could be due to the presence of MoO_2 oxide in the passive layer. The peak corresponding to that of 229.84 eV represents the higher oxidation state (6^+) of Mo, probably pertaining to $[MoO_4]^{2-}$. Similar compounds of Mo for Mo-3d were reported in the passive film analysis of Ni-based (Ni-Mo-Cr) and Fe-based alloys (SS316, SS304).[27–34]

Figure 12(c) shows XPS spectra of $Cr_{2p3/2}$, which is deconvoluted into three peaks having different B.E values.

The B.E of 575.93 eV could be assigned to Cr^{3+}.[31–34] The other peak at 572.31 eV is assigned to Cr^0 (metallic Cr) and the peak at 579.28 eV corresponds to Cr^{6+}.[27–30,33,34] Considering the individual contribution of each peak, this system possesses Cr^{3+} in maximum abundance (~82 pct), whereas the percentage of Cr^{6+} is the minimum (~1 pct). The unreacted Cr metal from the alloy present in the passive layer accounts to be (~17 pct). Thus, Cr is predominantly present as Cr^{3+}. The Cr^{3+} so found could be a mixture of both Cr_2O_3 and that of Cr $(OH)_3$ in the passive layer. This observation is also supported by the fact that the O-1s peak showed the presence of both lattice oxygen and hydroxide of alloying elements (Figure 12(a)).

XPS spectra of Si-2p peak are presented in Figure 12(d). Si XPS peak, as shown in Figure 12(d), is obtained at binding energy of 101.66 eV which corresponds to Si^{4+} as present in SiO_2.[35] Exact spin-orbit splitting of the Si-2p was not observed in this study because of use of a non-monochromatized source of Al Kα (1486.6 eV) with the best resolution of 0.89 eV, whereas the ΔE between the $Si\text{-}2p_{1/2}$ and $Si\text{-}2p_{3/2}$ is reported to be 0.6 eV with a FWHM of 0.65 eV.[36,37] The results obtained in the present study revealed that the passive film of laser clad layer of Ni-Mo-Cr-Si alloy in 0.5 M H_2SO4 at constant potential of ~0.6 V is predominantly composed of the oxides of elements such as Mo, Cr, and Si.

IV. DISCUSSION

Optimum processing parameters' window (Table II) at constant spot size of the laser beam (~2 mm) was established to produce crack- and porosity-free clad layer of Ni-Mo-Cr-Si, with low dilution (10 to 15 pct) and sound metallurgical bond with the SS316L substrate. A desirable dilution to the extent of maximum 3 to 10 pct is generally recommended[38] for a good quality clad layer deposited by laser cladding. Cracking at very low cladding speed (<100 mm/min) or high-powder feed rate (>20 gm/min) could be due to accumulation of large volume of Ni-Mo-Cr-Si alloy powder consisting of high fraction of hard intermetallic laves phase, which enhances the cracking tendency of this alloy. Tribaloy series of alloys contain a large volume fraction (~50 to 60 pct) of a hard, intermetallic laves phase in a relatively softer matrix.[10–12] These intermetallic phases are hard, but have limited amenability for plastic flow and have low fracture toughness,[39,40] which make them prone to cracking due to any stress generated during processing. Cracking at higher speed (>800 mm/min) could be attributed to increase in the temperature gradients and cooling rates. Generally temperature gradients and cooling rates tend to increase with increasing travel speed and correspondingly increase in the resulting internal stresses.[41,42]

Excellent corrosion resistance of Ni-Mo-Cr-Si alloy laser clad layer, in both reducing (0.1 M HCl) and oxidizing acid (0.5 M HNO_3) solutions can be attributed not only to the alloy chemistry which contains high Mo (~32 wt pct), Cr (~15 wt pct), and minor addition of Si (~3 wt pct), but also to the laser cladding process which produced a defect-free cladding while preserving chemistry of the additive alloy in the clad layer at optimized parameters. Nearly equal partitioning of Cr in both the phases (Table III) leads to overall good corrosion resistance of the alloy.

Higher pitting corrosion resistance of Ni-Mo-Cr-Si alloy laser clad layer as compared to the substrate SS316L, in HCl (reducing) acid environment, can be attributed to the much higher Mo (~32 wt pct) in the alloy as compared to that in SS316L (~2 to 3 wt pct), which resulted in faster repassivation kinetics in case of breakdown of the passive layer.[32,33] Hayes *et al.*[33] studied several Ni-Cr-Mo alloys in different acidic solutions including hydrochloric acid (HCl), sulfuric acid (H_2SO_4), nitric acid (HNO_3), hydrofluoric acid (HF), and phosphoric acid (H_3PO_4) to examine the complementary roles of chromium and molybdenum in nickel alloy passivation. The authors have shown that above a threshold Cr concentration (~11 pct), complete monolayer of chromium oxide passivates the surface of the alloy. The authors have also reported that with the increase in molybdenum content in these alloys, there was significant improvement in the repassivation behavior after breakdown occurred. In order to explain this behavior, it has been proposed that Mo preferentially partitions to local defects and slows the anodic dissolution because of its higher metal–metal bond strength.[27,31–34] In addition, it has also been proposed that MoO_4^{-2} forms in the solid state at the exterior

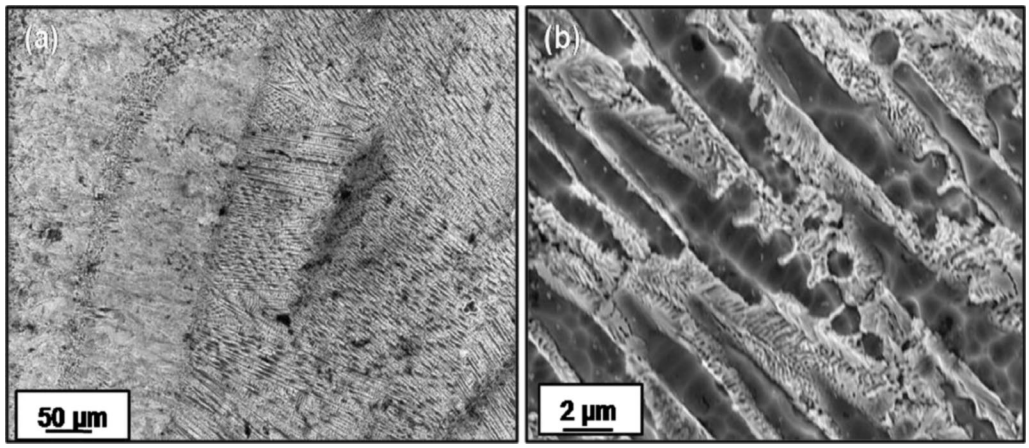

Fig. 8—SE (*a*) low and (*b*) high-magnification micrographs of laser clad Ni-Mo-Cr-Si alloy after electrochemical polarization in 0.5 M HNO_3, showing etched structure with selective dissolution of eutectic matrix or gamma solid solution phase (gray) as compared to Mo-rich intermetallic Laves phase.

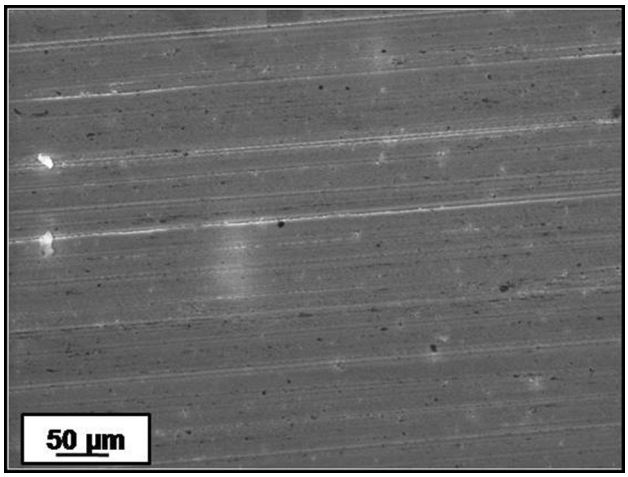

Fig. 9—SEM micrograph of SS316L after electrochemical polarization in 0.5 M HNO_3, showing a passivated and unattacked surface.

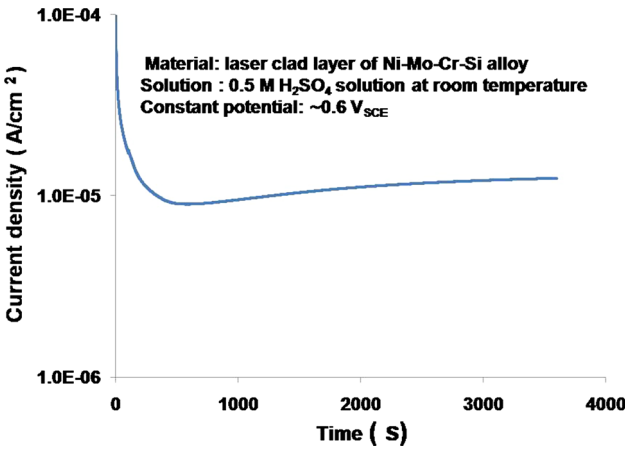

Fig. 10—Potentiostatic curve for laser clad layer of Ni-Mo-Cr-Si alloy, showing the passive film stability exposed at a potential of ~0.6 V_{SCE} (within the passive regime) in 0.5 M H_2SO_4 solution.

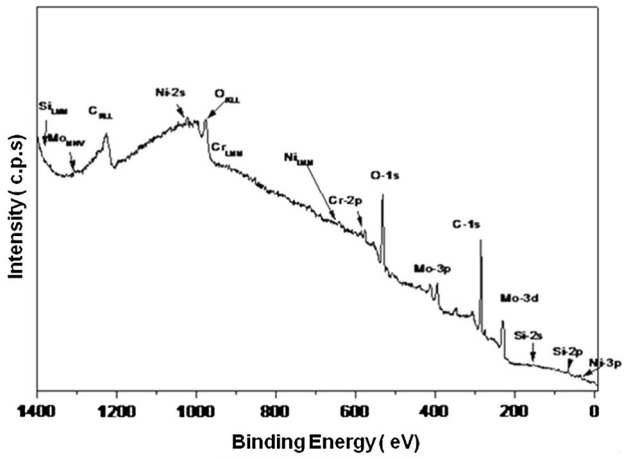

Fig. 11—XPS survey spectrum showing peaks of Ni-2p, Cr-2p, Mo-3p, Mo-3d, C-1s, O-1s and Si-2p, present in the passive layer formed on laser clad surface of Ni-Mo-Cr-Si alloy, electrochemically treated in 0.5 M H_2SO_4 at constant potential of ~0.6 V.

regions of the film, which is cation-selective, and resists incorporation of anions such as Cl^-, NO_3^-, and OH^-. This results in the growth of a Cr oxide in the inner barrier layer. The bipolar film thus formed stabilizes the passive oxide film and facilitates faster repassivation kinetics.[27] Several studies have also reported[43–45] the beneficial effect of Si in increasing the resistance to pitting corrosion due to the increased stability of the passive film, resulting from an increase in the Si content of the protective film.

Low and nearly identical corrosion current density (i_{corr}) values for both the laser clad Ni-Mo-Cr-Si alloy (1.48×10^{-7} A/cm^2) and the substrate SS316L (1.99×10^{-7} A/cm^2) in 0.1 M HCl environment indicated that the corrosion rates for these alloys are nearly same. This is due to the presence of high Cr content (>12 wt pct) in both of these alloys,[24] whereas the corrosion potential (E_{corr}) of laser clad layer showed higher active potential (−0.184 V_{SCE}) as compared to SS316L (−0.103 V_{SCE}) in the 0.1 M HCl solution. This

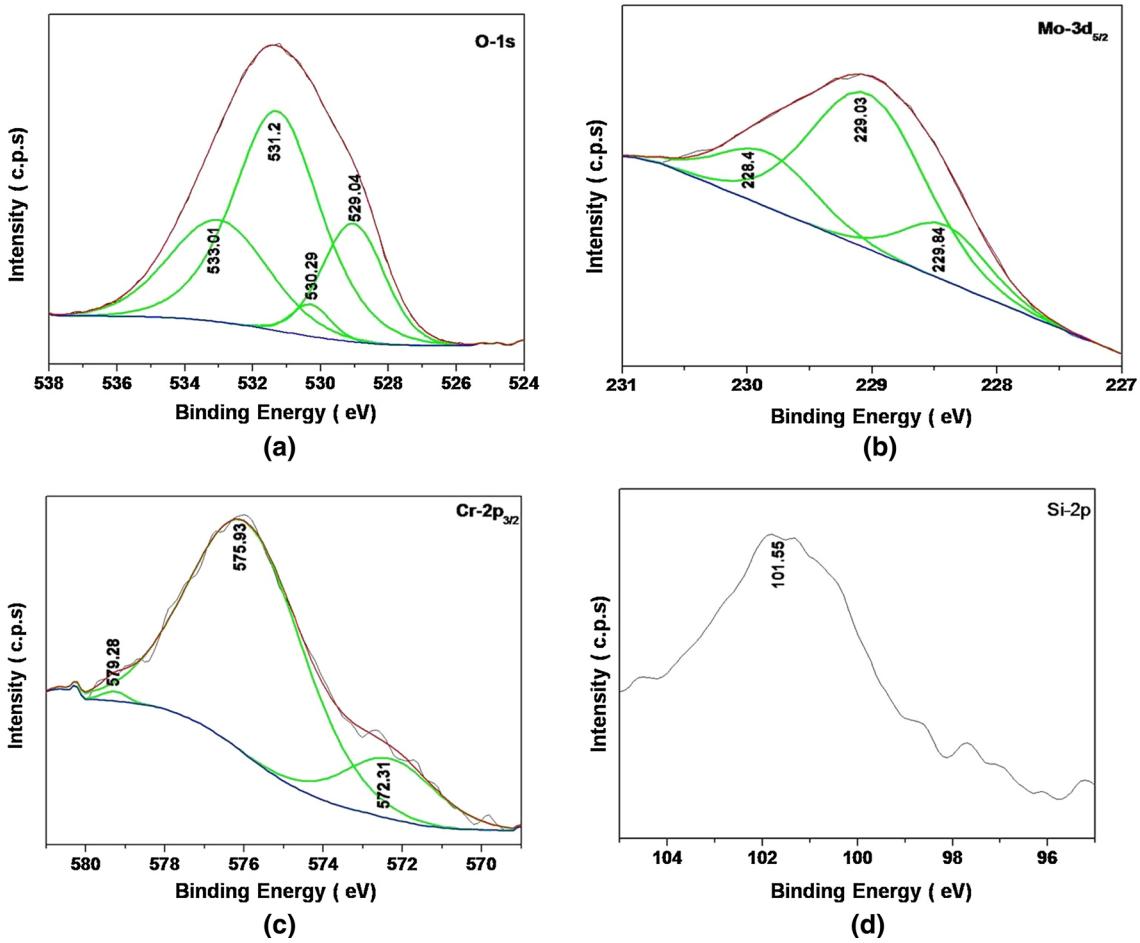

Fig. 12—(*a*) High-resolution XPS spectra of oxygen (O-1s), showing different oxides (531.2, 530.29, and 529.04 eV) and hydroxides (533.01 eV) of the alloying elements in the passive layer of laser clad Ni-Mo-Cr-Si alloy, exposed at a potential of ~0.6 V_{SCE} in 0.5 M H_2SO_4 solution. (*b*) High-resolution XPS spectra of molybdenum ($Mo_{3d5/2}$), showing different oxidation states of Mo (Mo^0 (228.4 eV) Mo^{+4} (229.03 eV) and Mo^{+6} (229.84 eV)) in the passive layer of laser clad Ni-Mo-Cr-Si alloy, exposed at a potential of ~0.6 V_{SCE} in 0.5 M H_2SO_4 solution. (*c*) High-resolution XPS spectra of chromium ($Cr_{2p3/2}$) showing different oxidation states of Cr [Cr^0 (572.31 eV), Cr^{3+} (575.93 eV) and Cr^{6+} (579.28 eV)] in passive layer of laser clad Ni-Mo-Cr-Si alloy, exposed at a potential of ~0.6 V_{SCE} in 0.5 M H_2SO_4 solution. High-resolution XPS spectra of Silicon (Si 2p) showing Si^{4+} oxidation states of Si in passive layer of laser clad Ni-Mo-Cr-Si alloy, exposed at a potential of ~0.6 V_{SCE} in 0.5 M H_2SO_4 solution.

difference in E_{corr} values can be attributed to the difference in microstructures of the two alloys. The inter-phase elemental partitioning in microstructure of an alloy affects the passive film stability across the metal surface.[24] The laser clad layer showed an inhomogeneous microstructure with dendrites and the matrix phases with some amount of elemental segregation in each phase (Table III). Therefore, the E_{corr} value in the case of laser clad layer would be determined by the relative dissolution kinetics of these phases in the environment and the ease with which the passive layer gets stabilized. In the case of SS316L, the microstructure being more homogenous (wrought microstructure) resulted in a nobler E_{corr} potential as compared to laser clad layer of Ni-Mo-Cr-Si alloy. The active potential is an indication of the microstructure playing a role in attaining the E_{corr} potential. E_{corr} value is governed anodically. This anodic controlled reaction results in a change in potential for both the alloys but the current density variation remains negligible.

Nearly similar corrosion behavior with higher breakdown or transpassive potential (~0.85 V_{SCE}), wide passivation range (~0.8 V_{SCE}), and low passive current density values (~4 to 7 × 10^{-6} A/cm^2) in both the laser clad layer and the substrate SS316L in HNO_3 (oxidizing) solution was due to oxidizing nature of NO_3^- ions which enhance the formation of a stable passive film on the surface.[24] While in HCl environment, Cl^- ions instead chemically alter and locally remove the passivation film, and thus promote pitting corrosion more specifically in case of SS316L substrate containing lower Mo content (~2 to 3 wt pct) than that of clad alloy (~32 wt pct). Additionally, Cl^- ions facilitate easy penetration into the minor defects in the passive layer, which often become preferential sites for initiation of pitting corrosion.

As mentioned above, the excellent corrosion resistance of laser clad layer of Ni-Mo-Cr-Si alloy was also primarily due to defect-free coating produced by laser cladding technique with optimized parameters.

Defect-free coating is one of the crucial requirements for improving corrosion behavior.[19] Defective coatings cannot exhibit excellent corrosion behavior in spite of deposition of the noblest alloy. This is evident from the fact that the coating of Tribaloy series of intermetallic alloy Ni-700 (Ni-Mo-Cr-Si) and also of T-800 (Co-Mo-Cr-Si) deposited by HVOF technique, showed[15,16] lack of passivation, exhibiting high passive current density (~10^{-4} A/cm^2) in both 0.1 M HCl and 0.5 M HNO_3 solutions, despite having high Mo and Cr concentrations. Thus, it did not display ideal perfect passive stage, which requires much lower current density ~10^{-6} A/cm^2. This lack of passivation and associated high corrosion current density of thermally sprayed coatings could be attributed to the presence of defects such as lamellae boundaries, porosities, unmelted particles, and oxide inclusions. These defects are generally inherent to thermally sprayed coatings and lead to infiltration of corrosive agents and impair the corrosion resistance of even the noblest alloy compositions.[46,47] These chemical inhomogeneities can also act as preferential sites for corrosion initiation, where galvanic coupling with the matrix results in pitting of the metal–oxide interface, in acidic environment. Thus, even though materials tend to passivate due to the presence of elements such as high Ni, Mo, and Cr, defects generally associated with the thermally sprayed coatings may act as corrosion initiation sites and alter the intrinsic corrosion resistance of the material. In contrast, laser-deposited clad layer in the present study exhibited passivity with low current density ~10^{-6} to 10^{-5} A/cm^2 and the absence of pitting after exposure in 0.1 M HCl. It also showed perfect passive stage with low current density ~4 to 7 × 10^{-6} A/cm^2 in 0.5 M HNO_3 solution. Only after polarization beyond breakdown potential (~0.8 V_{SCE}) in both reducing (0.1 M HCl) and oxidizing acid (0.5 M HNO_3) solutions, laser clad layer showed selective attack along the matrix (eutectic or gamma solid solution). This selective dissolution of matrix phase containing lesser Mo content as compared to Mo-rich intermetallic laves phase was due to the increased transpassive dissolution at high polarized potentials beyond passive region.

The XPS analysis of passive film formed on laser clad layer of Ni-Mo-Cr-Si alloy after exposure in 0.5 M H_2SO_4 at constant potential of ~0.6 V showed that the passive film was composed predominantly of the oxides of elements Mo, Cr, and Si. These oxides are formed from the dehydration of the hydroxide precursors which are direct result of the exposure to the 0.5 M H_2SO_4. The three different peaks of O-1s corresponding to different B.E values could be attributed to different proportions of elements in oxide, leading to different electronic environments and therefore peak positions. The passive film formed on laser clad layer of Ni-Mo-Cr-Si alloy has major contribution from Mo, present in different oxidation states as MoO_2 (Mo^{+4}) and $[MoO_4]^{-2}$ (Mo^{+6}). Mo^0 peaks are due to contributions from the substrate. As per one of the mechanisms proposed[27,31–34] for the role of Mo in improving the pitting corrosion resistance of Fe- and Ni-based alloys, the presence of Mo as $[MoO_4]^{2-}$ is expected at the outer regions of the oxide film. This acts as a cation getter and repels the negatively charged ions such as chloride, sulfate, and nitrate ions[27] from entering into the film. This imparts excellent passivation and repassivation characteristics to the alloy and thus increases passivity of the surface. The presence of Cr predominantly as Cr^{3+} (mixture of both Cr_2O_3 and that of Cr $(OH)_3$ in the passive layer) and Si, as Si^{4+}(SiO_2) might also have contributed to passive film formation and repassivation as also observed by other researchers.[28,33,43–45]

V. CONCLUSIONS

Laser clad layer of Ni-Mo-Cr-Si exhibited higher pitting corrosion resistance in 0.1 M HCl chloride (reducing) environment, indicated by higher breakdown potential (~0.8 V_{SCE}) and absence of pitting as compared to substrate SS316L (~0.3 V_{SCE}). However, in 0.5 M HNO_3 solution (oxidizing environment), both the laser clad layer and substrate SS316L exhibited excellent corrosion resistance exhibiting high breakdown potential (~0.85 V_{SCE}) and wide passivation range (~0.8 V_{SCE}) with low passive current density (4 to 7 × 10^{-6} A/cm^2). The passive layer formed on the laser clad layer of Ni-Mo-Cr-Si alloy after exposure in 0.5 M H_2SO_4 at constant potential ~0.6 V_{SCE} for 1 hour showed stable passive film containing oxides of Mo as Mo^{+4} (MoO_2) and Mo^{+6} $(MoO_4)^{-2}$, Cr as Cr^{3+} (mixture of both Cr_2O_3 and Cr $(OH)_3$) as well as Si as Si^{4+}(SiO_2). These oxides contributed to passive film formation, repassivation, and therefore excellent corrosion behavior.

REFERENCES

1. M.F. Ashby and D.R.H. Jones: *An introduction to Their Properties*, 1st ed., Pergamon Press, Butterworth-Heinemann, Oxford, 1987.
2. F.A. Crane and J.A. Charles: *Selection and Use of Engineering Materials*, Butterworth-Heinemann, Oxford, 1997.
3. Z.A. Foroulis: *Wear*, 1984, vol. 96, pp. 203–18.
4. J.R. Davis: *ASM* Handbook, ASM International, Materials Park, 2011, vol. 6, pp. 463–85.
5. D. Raghu and J.B.C. Wu: *Materials Performance*, 1997, vol. 36 (11), pp. 27–36.
6. R. Joseph: *Davis: tool materials, ASM speciality handbook*, ASM International, Materials Park, 1995.
7. R.D. Schmidt and D.P. Ferriss: *Wear*, 1975, vol. 32, pp. 279–89.
8. J.R. Devis: *Nickel, Cobalt, and Their Alloys, ASM Speciality Handbook*, ASM International, Materials Park, 2000.
9. J.J. Demo, D.P. Ferriss, Jr (1974) U.S. Patent, E. I. du Pont de Nemours and Company, Wilmington, DE, Patent No. 3,839,024.
10. A. Halstead and R.D. Rawlings: *Mater. Sci.*, 1984, vol. 18 (10), pp. 491–500.
11. S.E. Mason and R.D. Rawlings: *Mater. Sci. Technol.*, 1989, vol. 5, pp. 180–85.
12. R. Awasthi, S. Kumar, K. Chandra, B. Vishwanadh, R. Kishore, C.S. Viswanadham, D. Srivastava, and G.K. Dey: *Metall. Mater. Trans. A*, 2012, vol. 43A, pp. 4688–4702.
13. E.I. Landerman, D.J. Boes, P. Bowen, M.J. Huck (1984) EPRI Report, EPRI NP-3446.
14. R.N. Johnson: *Thin solid films*, 1984, vol. 118, pp. 31–47.
15. G. Bolelli, L. Lusvarghi, and R. Giovanardi: *Surf. Coat. Technol.*, 2008, vol. 202, pp. 4793–4809.

16. G. Bolelli, L. Lusvarghi, and M. Barletta: *Surf. Coat. Technol.*, 2008, vol. 202, pp. 4839–47.
17. R.N. Johnson and D.G. Farwick: *Thin Solid Films*, 1978, vol. 53, pp. 365–73.
18. D.G. Farwick and R.N. Johnson: *Thin Solid Films*, 1980, vol. 73, pp. 145–53.
19. B.C. Oberlander and E. Lugscheider: *Mater. Sci. Technol.*, 1992, vol. 8, pp. 657–65.
20. P.J.E. Monson and W.M. Steen: *Surf. Eng.*, 1990, vol. 6, pp. 185–94.
21. Z.Y. Al-Taha. Ph. D. Thesis, Dublin City University, 2008.
22. M.M. Rakhes. Ph. D Thesis, The University of Manchester, 2013.
23. E. Toysarkani, A. Khajepour, and S.F. Corbin: *Laser Cladding*, CRC Press, Boca Raton, 2004.
24. S.D. Cramer and B.S. Covino: *Corrosion: Fundamentals, Testing, and Protection. ASM Handbook*, ASM International, Materials Park, 2011.
25. N. Fairley: Casa XPS VAMAS Processing Software < http://www.casaxps.com/>.
26. D.A. Shirley: *Phys. Rev. B*, 1972, vol. 5, p. 4709.
27. C.R. Clayton and Y.C. Lu: *J. Electrochem. Soc.*, 1986, vol. 133 (12), pp. 2465–72.
28. X. Zhang, D. Zagidulin, and D.W. Shoesmith: *Electrochim. Acta*, 2013, vol. 89, pp. 814–22.
29. T. Hanawa, S. Hiromoto, A. Yamamoto, D. Kuroda, and K. Asami: *Mater. Trans.*, 2002, vol. 43 (12), pp. 3088–92.
30. R. Natarajan, N. Palaniswamy, M. Natesan, and V.S. Muralidharan: *Open Corros. J.*, 2009, vol. 2, pp. 114–24.
31. R.C. Newman: *Corros. Sci.*, 1985, vol. 25 (5), pp. 331–39.
32. C.A. Lloyd, J.J. Noel, S. McIntyre, and W.D. Shoesmith: *Electrochim. Acta*, 2004, vol. 49, pp. 3015–27.
33. J.R. Hayes, J.J. Gray, A.W. Szmodis, and C.A. Orme: *Corros. Sci.*, 2006, vol. 62 (6), pp. 491–500.
34. J.G. Choi and L.T. Thompson: *Appl. Surf. Sci.*, 1996, vol. 93, pp. 143–49.
35. A. Thogersen, J.H. Selj, and E.S. Marstein: *J. Electrochem. Soc.*, 2012, vol. 159 (5), pp. 276–81.
36. C.H.F. Peden, J.W. Rogers, N.D.S. Kidd, and K.L. Tsang: *Phys. Rev. B*, 1993, vol. 47, p. 1993.
37. F. Himpsel, F. McFeeley, A. Taleb-Ibrahimi, J. Yarmoand, and G. Hollinger: *Phys. Rev. B*, 1988, vol. 38, p. 6084.
38. J.R. Davis: *ASM Handbook*, ASM, Materials park, 1992, vol. 6, pp. 861–72.
39. A. Halstead and R.D. Rawlings: *J. Mater. Sci.*, 1985, vol. 20, pp. 1248–56.
40. W. Xu, R. Liu, P.C. Patnaik, M.X. Yao, and X.J. Wu: *Mater. Sci. Eng. A*, 2007, vol. 405, pp. 427–36.
41. K. Komvopoulos and K. Nagarathnam: *J. Eng. Mater. Technol.*, 1990, vol. 112, pp. 131–43.
42. R. Jendrzejewski, G. Sliwinski, M. Krawczuk, and W. Ostachowicz: *Comput. Struct.*, 2004, vol. 82, pp. 653–58.
43. I.H. Toor, J.Y. Kwon, and H.S. Kwon: *J. Electrochem. Soc.*, 2008, vol. 155 (9), pp. C495–C500.
44. F.H. Scott, G.C. Wood, and J. Stringer: *Oxid. Met.*, 1995, vol. 113, p. 45.
45. S.N. Basu and G.J. Yurck: *Oxid. Met.*, 1991, vol. 281, p. 315.
46. D. Zhang, S.J. Harris, and D.G. McCartney: *Mater. Sci. Eng. A*, 2003, vol. 344, pp. 45–56.
47. W.M. Zhao, Y. Wang, L.X. Dong, K.Y. Wu, and J. Xue: *Surf. Coat. Technol.*, 2005, vol. 190, pp. 293–98.